

Rethinking Semi-Supervised Medical Image Segmentation: A Variance-Reduction Perspective

Chenyu You¹, Weicheng Dai², Yifei Min¹, Fenglin Liu³, Xiaoran Zhang¹,
David A. Clifton³, S. Kevin Zhou⁴, Lawrence Staib¹, James S. Duncan¹

¹Yale University ²New York University ³University of Oxford

⁴University of Science and Technology of China

chenyu.you@yale.edu

Abstract

For medical image segmentation, contrastive learning is the dominant practice to improve the quality of visual representations by contrasting semantically similar and dissimilar pairs of samples. This is enabled by the observation that without accessing ground truth label, negative examples with truly dissimilar anatomical features, if sampled, can significantly improve the performance. In reality, however, these samples may come from similar anatomical features and the models may struggle to distinguish the minority tail-class samples, making the tail classes more prone to misclassification, both of which typically lead to model collapse. In this paper, we propose **ARCO**, a semi-supervised contrastive learning (CL) framework with stratified group sampling theory in medical image segmentation. In particular, we first propose building **ARCO** through the concept of variance-reduced estimation, and show that certain variance-reduction techniques are particularly beneficial in medical image segmentation tasks with extremely limited labels. Furthermore, we theoretically prove these sampling techniques are universal in variance reduction. Finally, we experimentally validate our approaches on three benchmark datasets with different label settings, and our methods consistently outperform state-of-the-art semi-supervised methods. Additionally, we augment the CL frameworks with these sampling techniques and demonstrate significant gains over previous methods. We believe our work is an important step towards semi-supervised medical image segmentation by quantifying the limitation of current self-supervision objectives for accomplishing medical image analysis tasks.

ical segmentation models. The success of traditional supervised learning depends on training deep networks on a large amount of labeled data, but this improved model robustness often comes at the cost of annotations and clinical expertise [36, 62, 86]. Therefore, it is difficult to adopt these models in real-world clinical applications.

Recently, a significant amount of research efforts [4, 48, 52, 76, 89, 96, 97] have resorted to unsupervised or semi-supervised learning techniques for improving the segmentation robustness. One of the most effective methods is *contrastive learning* (CL) [21, 39, 41, 59]. It aims to learn useful representations by contrasting semantically similar (*positive*) and dissimilar (*negative*) pairs of data points sampled from the massive unlabeled data. These methods fit particularly well with the real-world clinical scenarios as we assume only access to a large amount of unlabelled data coupled with extremely limited labels. However, pixel-level contrastive learning with medical images segmentation is quite impractical since sampling all pixels can be extremely time-consuming and computationally expensive. Fortunately, recent studies [84, 85] provide a remedy by leveraging the bootstrapping strategy, which first actively samples a sparse set of pixel-level representations, and then learns anatomically meaningful features in a contrastive optimization objective. In particular, it jointly addresses the *imbalancedness* (*i.e.*, imbalanced class distribution) and *diversity* (*i.e.*, intra-slice correlations within the entire dataset) issues, unleashing the potential of utilizing massive unlabeled data with extremely limited annotations while maintaining impressive segmentation performance compared to supervised counterparts. Meanwhile, it can lead to substantial memory/computation reduction when using pixel-level CL framework for medical segmentation.

1. Introduction

Model robustness and label efficiency are two highly desirable perspectives when it comes to building reliable med-

Nevertheless, in practical clinical settings, the deployed CL models often ask for strong model robustness, *i.e.*, being robust against the *collapse* problems whereby all representations collapse into constant features [5, 21, 23, 41, 71, 90]

or only span a lower-dimensional subspace [43, 45, 70, 87]. Therefore, a more challenging requirement arises, which is far beyond the scope of segmentation quality especially for such safety-critical scenarios. One blessing comes from the recent empirical finding in the context of image classification [44], which suggests that one cause of such fragility could be attributed to the non-smooth feature space near samples, *i.e.*, **random sampling from bootstrapping can result in large feature variations**. Thus, it is a new perspective: *towards improving variance reduction in training semi-supervised contrastive learning models*. This inspires us to propose a new hypothesis of semi-supervised contrastive learning. Specifically, when directly baking in variance-reduction techniques into semi-supervised contrastive learning framework for medical image segmentation, the models can further push toward the state-of-the-art segmentation robustness and label efficiency.

In this paper, we present **ARCO**, a semi-supervised stratified group contrastive learning framework with two perspectives (*i.e.*, **model robustness** and **label efficiency**), and with the aid of variance-reduction estimation, realize two practical solutions – Stratified Group (SG) and Stratified-Antithetic Group (SAG) – for selecting the most semantically informative pixels. ARCO is a group-based sampling method that builds a set of pixel groups and then proportionally samples from each group with respect to the class distribution. The main approach we take for building our proposed ARCO is via first partitioning the image into grids with the same size, and then sampling, within the same grid, the pixels semantically close to each other with high probability, with minimal additional memory footprint.

Subsequently, we show that baking ARCO into contrastive pre-training (*i.e.*, MONA [84]) provides an efficient pixel-wise contrastive learning paradigm to train deep networks that generalize well beyond training data. ARCO is easy to implement, being built on top of off-the-shelf pixel-level contrastive learning framework [5, 21, 37, 41, 69], and consistently improves overall segmentation quality across all label ratios and datasets.

Our analysis shows that, ARCO is more label efficient, providing practical means for computing the gradient estimator with a reduced variance. Empirically, our approach significantly improves over the state-of-the-art across three medical image segmentation benchmarks. Our proposed framework has several theoretical and practical contributions:

- We propose ARCO, a new CL framework based on stratified group sampling theory to improve the label efficiency and model robustness trade-off in CL for medical segmentation. We show that incorporating ARCO coupled with two special sampling methods, such as Stratified Group and Stratified-Antithetic Group, into the models provides an efficient learning

paradigm to train deep networks that generalize well beyond training data in those long-tail clinical scenarios.

- To the best of our knowledge, we are the **first work** to show the benefit of certain variance-reduction techniques in contrastive learning for medical image segmentation. We demonstrate the unexplored advantage of the refined gradient estimator in handling medical image data from imbalanced and diverse distributions.
- We conduct extensive experiments to validate the effectiveness of our proposed method using a variety of datasets, network architectures, and different label ratios. For segmentation robustness, we show that our proposed method by demonstrating the superior segmentation accuracy on all three benchmark datasets.
- We provide a theoretical analysis of ARCO with reduced variance and optimization guarantees. We further demonstrate the intriguing property of ARCO in the different pixel-level contrastive learning frameworks.

2. Related work

Medical Image Segmentation. Contemporary medical image segmentation approaches typically build upon fully convolutional networks (FCN) [51] or UNet [64], which formulates the task as a dense classification problem. In general, current medical image segmentation methods can be cast into two sets: network design and optimization strategy. One is to optimize segmentation network design for improving feature representations through dilated/atrous/deformable convolutions [19, 20, 27], pyramid pooling [18, 33, 94], multi-scale contexts [77, 78], and attention mechanisms [38, 57, 58]. Most recent works [13, 17, 40, 72, 82, 86] reformulate the task as a sequence-to-sequence prediction task by using the vision transformer (ViT) architecture [28, 73]. The other is to improve optimization strategies, by designing loss function to better address class imbalance [50] or refining uncertain pixels from high-frequency regions improving the segmentation quality [67, 83, 88]. In contrast, we take a leap further to a more practical clinical scenario by leveraging the massive unlabeled data with extremely limited labels in the learning stage. Moreover, we focus on building a *model-agnostic*, label-efficient framework to improve segmentation quality by providing additional supervision on the most confusing pixels for each class. In this work, we question how medical segmentation models behave under such diverse and imbalanced data and whether they can generalize well in those challenging scenarios through sampling methods.

Semi-Supervised Learning (SSL). SSL aims to train models with a combination of labeled, weakly-labeled and

unlabelled data. In recent years, there has been a surge of work on semi-supervised medical segmentation [4, 12, 14, 24, 29, 34, 46, 48, 54, 56, 76, 84, 85, 88, 89, 92], which makes it hard to present a complete overview here. We therefore only outline some key milestones related to this study. In general, it can be roughly categorized into two groups: (1) Consistency regularization was first proposed by [3], which aims to impose consistency corresponding to different perturbations into the training, such as consistency regularization [10, 26, 30, 31, 35, 96], pi-model [65], co-training [61, 97], and mean-teacher [49, 63, 68]. (2) Self-training was initially proposed in [66], which aims at using a model’s predictions to obtain noisy pseudo-labels for performance boosts with minimal human labor, such as pseudo-labeling [4, 24, 29, 48], model uncertainty [12, 14, 34, 46, 54, 56, 89, 92], confidence estimation [9, 32, 47], and noisy student [80]. These methods usually lead to competitive performance but fail to prevent *collapse* due to class imbalance. In this work, we focus on semi-supervised medical segmentation with extremely limited labels since the medical image data is extremely diverse and often long-tail distributed over anatomical classes. We speculate that a good medical segmentation model is expected to distinguish the minority tail-class samples and hence achieve better performance under additional supervision on hard pixels.

Contrastive Learning. The past five years have seen tremendous progress related to CL in medical image segmentation [15, 16, 42, 79, 81, 84, 85, 87, 88, 91], and it becomes increasingly important to improve representation in label-scarcity scenarios. The key idea in CL [21, 39, 41, 59] is to learn representations from unlabeled data that obey similarity constraints by pulling augmented views of the same samples closer in a representation space, and pushing apart augmented views of different samples. This is typically achieved by encoding a view of a data into a single global feature vector. However, the *global representation* is sufficient for simple tasks like image classification, but does not necessarily achieve decent performance, especially for more challenging dense prediction tasks. On the other hand, several works on *dense contrastive learning* [15, 42, 87], aim at providing additional supervision to capturing intrinsic spatial structure and fine-grained anatomical correspondence, while these methods may suffer from *class imbalance* issues. Particularly, very recent work [84, 85] for the first time demonstrates the imbalancedness phenomenon can be mitigated by performing contrastive learning yet lacking stability. By contrast, a key motivation of our work is to bridge the connection between model robustness and label efficiency, which we believe is an important and under-explored area. We hence focus on variance-reduced estimation in medical image segmentation, and show that certain variance-reduction techniques can help provide more efficient approaches or alternative so-

lutions for handling *collapse* issues, and improving model robustness in terms of accuracy and stability. To the best of our knowledge, we are the first to provide a theoretical guarantee of robustness by using certain variance-reduction techniques.

3. Methodology

In this section we set-up our semi-supervised medical segmentation problem, introduce key definitions and notations and formulate an approach to incorporate stratified group sampling theory. Then, we discuss how our proposed ARCO can directly bake in two perspectives into deep neural networks: (1) **model robustness**, and (2) **label efficiency**.

3.1. Preliminaries and setup

Problem Definition. In this paper, we consider the same medical image segmentation problem setup as in MONA. Specifically, given a medical image dataset $(\mathcal{X}, \mathcal{Y})$, we wish to automatically learn a segmentator, which assigns each pixel to their corresponding K -class segmentation labels.

Setup. Contrastive learning aims to learn effective representations by pulling semantically close neighbors together and pushing apart other non-neighbors [39]. Among various popular contrastive learning frameworks, MONA [84] is easy-to-implement while yielding the state-of-the-art performance for semi-supervised medical image segmentation so far. The main idea of MONA is to discover diverse views (*i.e.*, augmented/mined views) whose anatomical feature responses are *homogeneous* within the same or different occurrences of the *same class type*, while at the same time being *distinctive* for *different class types*. We hence build our ARCO on the top of the MONA pipeline [84] for deriving the **model robustness** and **label efficiency** properties of our medical segmentation model. Figure 1 in Appendix overviews the high-level workflow of the proposed ARCO framework. In the following, we provide a concise overview of ARCO, consisting of two training phases: (1) relational semi-supervised pre-training, and (2) anatomical contrastive fine-tuning.

Let us denote \mathbf{x} as the input sample of the *student* and *teacher* networks $F(\cdot)$ ¹, consisting of an encoder E and a decoder D , and F is parameterized by weights θ_s and θ_t .

(1) Relational Semi-Supervised Pretraining. Given an unlabeled sample, ARCO has two ways to define *augmented* and *mined* views: (1) ARCO augments the samples to be \mathbf{x}^1 and \mathbf{x}^2 as *augmented* views, with two separate data augmentation operators; and (2) ARCO randomly samples d *mined* views (*i.e.*, \mathbf{x}^3) from the unlabeled dataset with additional augmentation. The pairs $[\mathbf{x}^1, \mathbf{x}^2]$ are then

¹The student and teacher networks both adopt the UNet design [64]

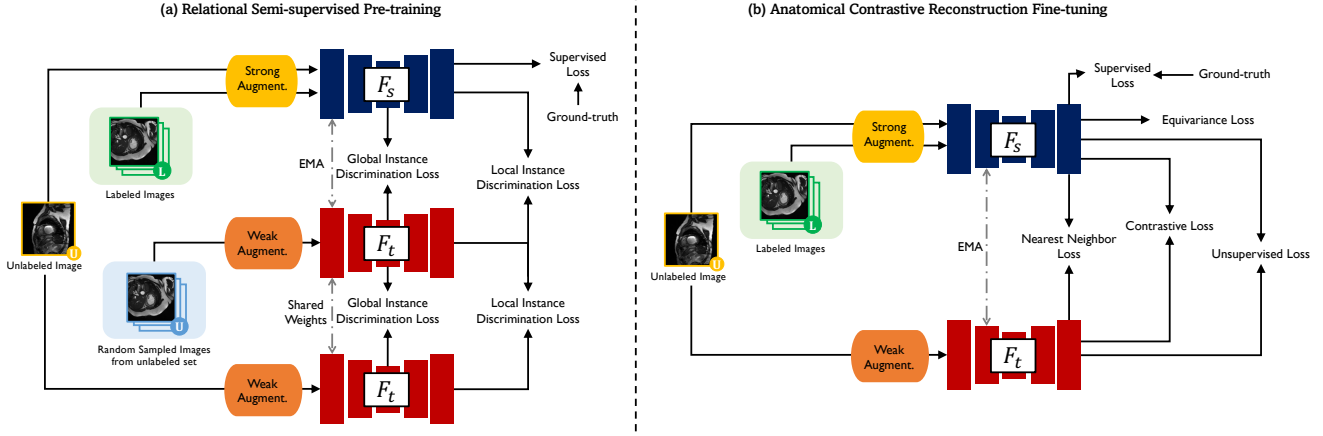


Figure 1. **Pipeline overview.** Our semi-supervised segmentation model F takes an 2D medical image x as input and outputs the segmentation map and the representation map. We leverage MONA pipeline [84] which is composed of two stages: (1) relational semi-supervised pre-training: on labeled data, the student network is trained by the ground-truth labels with the supervised loss \mathcal{L}_{sup} ; while on unlabeled data, the student network takes the *augmented* and *mined* embeddings from the EMA teacher for instance discrimination $\mathcal{L}_{\text{inst}}$ in the global and local manner, (2) our proposed anatomical contrastive reconstruction fine-tuning: on labeled data, the student network is trained by the ground-truth labels with the supervised loss \mathcal{L}_{sup} ; while on unlabeled data, the student network takes the representation maps and pseudo labels from the EMA teacher to give more importance to tail class $\mathcal{L}_{\text{contrast}}$, capture anatomical consistency \mathcal{L}_{eqv} , exploit the inter-instance relationship \mathcal{L}_{nn} , and compute unsupervised loss $\mathcal{L}_{\text{unsup}}$. See Appendix E.2 for details of the visualization loss landscapes.

processed by $[F_s, F_t]$, and in a similar way \mathbf{x}^3 is processed by F_s (See Figure 1(a) in Appendix), outputting three global features $[\mathbf{h}^1, \mathbf{h}^2, \mathbf{h}^3]$ after E and their local features $[\mathbf{f}^1, \mathbf{f}^2, \mathbf{f}^3]$ after D . These features are fed to the two-layer non-linear projectors for outputting global and local embeddings \mathbf{v}_g and \mathbf{v}_l .

To alleviate the *collapse* issues [37, 69, 85], we make the architecture asymmetric between the *student* and *teacher* pipeline by further feeding both the global and local embeddings \mathbf{v} with respect to the *student* branch into the non-linear predictor, producing \mathbf{w} in both global and local manners². After passing through the non-linear projectors and predictor, the relational similarities between *augmented* and *mined* embeddings are computed using the softmax transform, which can be formulated as: $\mathbf{u}_s = \log \frac{\exp(\text{sim}(\mathbf{w}^1, \mathbf{v}^3)/\tau_s)}{\sum_{n=1}^N \exp(\text{sim}(\mathbf{w}^1, \mathbf{v}_n^3)/\tau_s)}$, $\mathbf{u}_t = \log \frac{\exp(\text{sim}(\mathbf{w}^2, \mathbf{v}^3)/\tau_t)}{\sum_{n=1}^N \exp(\text{sim}(\mathbf{w}^2, \mathbf{v}_n^3)/\tau_t)}$, where τ_s and τ_t are different temperature parameters. The unsupervised instance discrimination loss (*i.e.*, Kullback-Leibler divergence \mathcal{KL}) can be defined as:

$$\mathcal{L}_{\text{inst}} = \mathcal{KL}(\mathbf{u}_s || \mathbf{u}_t). \quad (3.1)$$

The parameters of the *teacher* model are the exponential moving average (EMA) of the *student* model parameters that are updated by the stochastic gradient descent. For

²We omit details of local instance discrimination setting for simplicity in following contexts.

pretraining, the entire loss consists of the global and local instance discrimination loss, and supervised segmentation loss \mathcal{L}_{sup} (*i.e.*, equal combination of Dice loss and cross-entropy loss), *i.e.*, $\mathcal{L} = \mathcal{L}_{\text{inst}}^{\text{global}} + \mathcal{L}_{\text{inst}}^{\text{local}} + \mathcal{L}_{\text{sup}}$.

(2) Anatomical Contrastive Finetuning (ACF). We use the pre-trained network weights as the initialization for subsequent fine-tuning (See Figure 1(b) in Appendix). For semi-supervised training, we follow three principles described in [84]: (1) *tailness*: giving more importance to tail class hard pixels; (2) *consistency*: enforcing the feature invariances to specified data transformations; and (3) *diversity*: ensuring anatomical diversity in the set of different sampled images.

Following the abovementioned principles, we employ a three-step routine: (1) *tailness*: we first perform anatomical contrastive formulation. Specifically, we additionally attach the representation head ψ_r ³, and generate a higher n -dimensional dense representation with the same spatial resolution as the input image. A pixel-level contrastive loss is designed to pull queries $\mathbf{r}_q \in \mathcal{R}$ to be similar to the positive keys $\mathbf{r}_k^+ \in \mathcal{R}$, and push apart the negative keys $\mathbf{r}_k^- \in \mathcal{R}$.

³The representation head is only applied during training, and is removed during inference

The semi-supervised contrastive loss $\mathcal{L}_{\text{contrast}}$ is defined as:

$$\mathcal{L}_{\text{contrast}} = \sum_{c \in \mathcal{C}} \sum_{\mathbf{r}_q \sim \mathcal{R}_q^c} -\log \frac{\exp(\mathbf{r}_q \cdot \mathbf{r}_k^{c,+} / \tau)}{\exp(\mathbf{r}_q \cdot \mathbf{r}_k^{c,+} / \tau) + \sum_{\mathbf{r}_k^- \sim \mathcal{R}_k^c} \exp(\mathbf{r}_q \cdot \mathbf{r}_k^- / \tau)}, \quad (3.2)$$

where \mathcal{C} is a set including all available classes in the current mini-batch, and τ is a temperature hyperparameter. We refer to $\mathcal{R}_q^c, \mathcal{R}_k^c, \mathbf{r}_k^{c,+}$ as a query set including all representations within this class c , a negative key set including all representations whose labels is not in class c , and the positive key which is the c -class mean representation, respectively. Consider \mathcal{P} is a set including all pixel coordinates with the same resolution as R , these queries and keys are then defined as: $\mathcal{R}_q^c = \bigcup_{[i,j] \in \mathcal{A}} \mathbb{1}(\mathbf{y}_{[i,j]} = c) \mathbf{r}_{[i,j]}$, $\mathcal{R}_k^c = \bigcup_{[i,j] \in \mathcal{A}} \mathbb{1}(\mathbf{y}_{[i,j]} \neq c) \mathbf{r}_{[i,j]}$, $\mathbf{r}_k^{c,+} = \frac{1}{|\mathcal{R}_q^c|} \sum_{\mathbf{r}_q \in \mathcal{R}_q^c} \mathbf{r}_q$. (2) *consistency*: we then construct a set of random image transformation (*i.e.*, affine, intensity, and photo-metric augmentations), and define the semi-supervised equivariance loss \mathcal{L}_{eqv} by minimizing the symmetrized \mathcal{KL} divergence between the original mask and mask generated from the transformed image. (3) *diversity*: lastly, we leverage the first-in-first-out (FIFO) memory bank [41] to search for K -nearest neighbors, and use the semi-supervised nearest neighbor loss \mathcal{L}_{nn} in a way that maximizing cosine similarity, to exploit the inter-instance relationship.

For fine-tuning, the total loss includes contrastive loss $\mathcal{L}_{\text{contrast}}$, equivariance loss \mathcal{L}_{eqv} , nearest neighbors loss \mathcal{L}_{nn} , unsupervised cross-entropy loss $\mathcal{L}_{\text{unsup}}$ and supervised segmentation loss \mathcal{L}_{sup} : $\mathcal{L}_{\text{sup}} + \lambda_1 \mathcal{L}_{\text{contrast}} + \lambda_2 \mathcal{L}_{\text{eqv}} + \lambda_3 \mathcal{L}_{\text{unsup}} + \lambda_4 \mathcal{L}_{\text{nn}}$. See the Appendix E.4 for an ablation study of hyperparameters.

3.2. Motivation and Challenges

Intuitively, the contrastive loss will learn generalizable, balanced and diverse representations for downstream medical segmentation tasks if the positive and negative pairs correspond to the desired latent anatomical classes [15, 84, 85]. Yet, one critical constraint in real-world clinical scenarios is severe *memory bottlenecks* [55, 85]. To address this issue, current pixel-level CL approaches [84, 85] for high-resolution medical images devise their aggregation rules by *unitary simulators*, *i.e.*, *Naïve Sampling* (NS), that determines the empirical estimate from all available pixels. Despite the blessing of large learning capacity, such aggregation rules are *unreliable* “black boxes”. It is never well understood which rule existing CL models should use for improved **model robustness** and **label efficiency**; nor is it easy to compare different models and assess the model performance. Moreover, unitary simulators, especially naïve sampling, often incur high variances and fail to identify

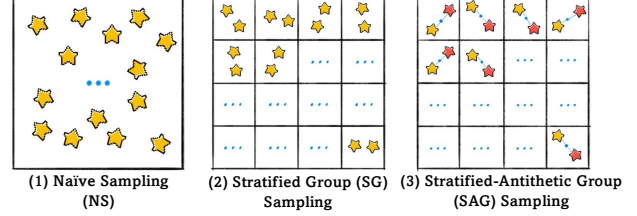


Figure 2. Overview of three sampling methods. (1) Naïve Sampling, (2) Stratified Group Sampling, and (3) Stratified-Antithetic Group Sampling.

semantically similar pixels [44], limiting CL stability. As demonstrated in Figure 3, regions of similar anatomical features should be grouped together in the original medical images, resulting in corresponding plateau regions in the visualization of the loss landscape. This is consistent with the observations uncovered by the recent empirical findings [22, 95].

If we take a unified mathematical perspective, the execution of simulation can be represented either through an *adaptive* rule, or by a *unitary* simulation. To tackle the two critical issues, we look back at adaptive rules. We hence propose two straightforward yet effective techniques – Stratified Group (SG) and Stratified-Antithetic Group (SAG) – to mitigate the undesirable high-variance limitation, and turn to the following idea of sampling the most representative pixels from groups of semantically similar pixels. In particular, our proposed solution is based on stratified group simulation to adaptively characterize anatomical regions found on different medical images. This characterization is succinct, and regions with the same anatomical properties within different medical images are identifiable. In practice, we first partition the image into grids with the same size, and then sampling, within the same grid, the pixels semantically close to each other with high probability, with minimal additional memory footprint (Figure 2).

In what follows, we will theoretically demonstrate the important properties of such techniques (*i.e.*, SG and SAG), especially in reduced variance and unbiasedness. Here the reduced variance implies more robust gradient estimates in the backpropagation, and leads to faster and stabler training in theory, as corroborated by our experiments (Section 4). Empirically, we will demonstrate many practical benefits of reduced variances including improved model robustness, *i.e.*, faster convergence and better segmentation quality, through mitigating the *collapse* issue.

3.3. Stratified Group Sampling

To be consistent with the previous notation, we denote an arbitrary image from the given medical image dataset as $\mathbf{x} \in \mathcal{X}$, and \mathcal{P} as the set of pixels. For arbitrary function

$h : \mathcal{X} \times \mathcal{P} \rightarrow \mathbb{R}$, we define the aggregation function H^4 as:

$$H(\mathbf{x}) = \frac{1}{|\mathcal{P}|} \sum_{p \in \mathcal{P}} h(\mathbf{x}; p). \quad (3.3)$$

As a large cardinality of \mathcal{P} prevents efficient direct computation of $H(\mathbf{x})$, an immediate approach is to compute $H(\mathbf{x})$ by first sampling a subset of pixels $\mathcal{D} \subseteq \mathcal{P}$ according to certain sampling strategy, and then computing $\hat{H}(\mathbf{x}; \mathcal{D}) = \sum_{p \in \mathcal{D}} h(\mathbf{x}; p) / |\mathcal{D}|$. SG sampling achieves this by first decomposing the pixels into M disjoint groups \mathcal{P}_m satisfying $\cup_{m=1}^M \mathcal{P}_m = \mathcal{P}$, and then sampling $\mathcal{D}_m \subseteq \mathcal{P}_m$ so that $\mathcal{D} = \cup_{m=1}^M \mathcal{D}_m$. The SG sampling can then be written as:

$$\hat{H}_{\text{SG}}(\mathbf{x}; \mathcal{D}) = \sum_{m=1}^M \frac{|\mathcal{P}_m|}{|\mathcal{P}|} \cdot \left(\frac{1}{|\mathcal{D}_m|} \sum_{p \in \mathcal{D}_m} h(\mathbf{x}; p) \right).$$

SAG, built upon SG, adopts a similar form, except for an additionally enforced symmetry on \mathcal{D}_m : $\forall m$, there exists some c_m such that for any $p \in \mathcal{D}_m$, there exists some corresponding $p' \in \mathcal{D}_m$ satisfying

$$c_m - p = p' - c_m.$$

Here c_m denotes the center of the group \mathcal{P}_m .⁵ The implementation of SG and SAG involves two steps: (1) to create groups $\{\mathcal{P}_m\}_{m=1}^M$, and (2) to generate each $\mathcal{D}_m \subseteq \mathcal{P}_m$. For the latter, we consider independent sampling within and between groups, i.e., $\mathcal{D}_m \perp \mathcal{D}_{m'}$ for $m \neq m'$, and $p \perp p' \forall p, p' \in \mathcal{D}_m$. The variance of such sampling is as follows.

Lemma 3.1. *Suppose in SG sampling, for each m , \mathcal{D}_m is sampled from \mathcal{P}_m with sampling variance σ_m^2 and sample size $|\mathcal{D}_m| = n_m$, with $n = \sum_{m=1}^M n_m$. Then the variance satisfies $\text{Var}[\hat{H}_{\text{SG}}] = \sum_{m=1}^M \sigma_m^2 n_m / n^2$, and SAG with the same sample size satisfies $\text{Var}[\hat{H}_{\text{SAG}}] \leq 2 \text{Var}[\hat{H}_{\text{SG}}]$.*

To ensure the unbiasedness property, we adopt the setting of proportional group sizes [2, 25], i.e., $|\mathcal{D}_m| \propto |\mathcal{P}_m|$ for all m . It turns out that such setting also brings the variance-reduction property.

Theorem 3.2 (Unbiasedness and Variance of SG). *SG with proportional group sizes is unbiased, and has a variance no larger than that of NS. That is: $\mathbb{E}[\hat{H}_{\text{SG}}(\mathbf{x})] = H(\mathbf{x})$, and*

$$\text{Var}[\hat{H}_{\text{SG}}] = \text{Var}[\hat{H}_{\text{NS}}] - \frac{1}{n} \sum_{m=1}^M \frac{n_m}{n} \left(\mathbb{E}_{p \sim \text{unif. } \mathcal{P}_m} [h(\mathbf{x}; p)] - \mathbb{E}_{p \sim \text{unif. } \mathcal{P}} [h(\mathbf{x}; p)] \right)^2.$$

⁴The pixel-level contrastive loss $\mathcal{L}_{\text{contrast}}$ is an example of an aggregation function (up to normalizing constant) according to (3.2).

⁵The choice of c_m is flexible. For example, if the convex hull of the pixels in \mathcal{P}_m form a circle, then c_m can be taken as the geometric center.

The last term is the intra-group variance, which captures the discrepancy between the pixel groups $\{\mathcal{P}_m\}_{m=1}^M$. Theorem 3.2 guarantees that the variance of SG is upper bounded by that of NS, and SG has strictly less variance than NS as long as all the pixel groups do not share an equal mean over $h(\mathbf{x}; p)$, which is almost-sure in medical images (See Figure 3). For SAG, Lemma 3.1 guarantees its variance is of the same magnitude as that of SG, and at worst differs by a factor of 2. Since the contrastive loss $\mathcal{L}_{\text{contrast}}$ is an aggregation function over pixels by definition (3.2), it benefits from the variance-reduction property of SG/SAG. In Section 4.1, we will see that such variance reduction allows ARCO to achieve better segmentation accuracy, especially along the boundary of the anatomical regions (Figure 4).

Training Convergence. The variance reduction estimation has additional benefit in terms of training stability. Specifically, leveraging techniques from optimization theory [1, 7, 11] we can show that variance-reduced gradient estimator through SG sampling leads to faster convergence in training. Suppose we have a loss function $\mathcal{L}(\theta)$ with the model parameter θ , and use stochastic gradient descent (SGD) as the optimizer. A gradient estimate $g(\theta) \approx \nabla \mathcal{L}(\theta)$ is computed at each iteration. It is well-known that the convergence of SGD depends on the quality of the estimate $g(\theta)$ [7]. Specifically, we make the common assumptions that the loss function is smooth and the gradient estimate has bounded variance (more details in Appendix A.3), which can be formulated as below:

$$\begin{aligned} \|\nabla \mathcal{L}(\theta) - \nabla \mathcal{L}(\theta')\|_2 &\leq L(\|\theta - \theta'\|_2), \\ \mathbb{E} \left[\|g(\theta) - \nabla \mathcal{L}(\theta)\|^2 \right] &\leq \sigma_g^2. \end{aligned}$$

Under these two assumptions, the average expected gradient norm of the objective function satisfies the following:

$$\frac{1}{T} \sum_{t=1}^T \mathbb{E} \left[\|\nabla \mathcal{L}(\theta_t)\|_2^2 \right] \leq C \left(\frac{1}{T} + \sqrt{\frac{\sigma_g^2}{T}} \right).$$

Under the non-convex optimization setting, the above implies convergence to some local minimum of the loss function. Importantly, the slow rate ($\sqrt{\sigma_g^2/T}$) depends on the variance σ_g^2 , indicating a faster convergence can be achieved with a more accurate gradient estimate. In Figure 5, we verify that using SG enables faster loss decay with smaller error bar, showing that it outperforms other methods in both the convergence speed and the stability. See Section 4.2 and Appendix A.3 for more details.

4. Experiments

In this section, we present experiment results to validate our proposed methods across various datasets and different

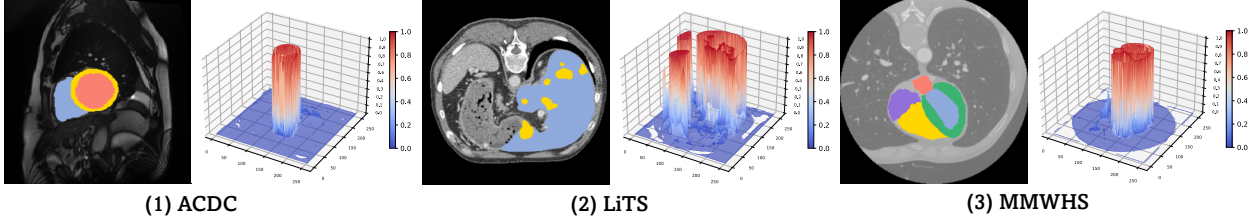


Figure 3. Loss landscape visualization of pixel-wise contrastive loss $\mathcal{L}_{\text{contrast}}$ with ARCO-SG. Loss plots are generated with same original images randomly chosen from ACDC [6], LiTS [8], and MMWHS [98], respectively. z -axis denotes the loss value at each pixel. For each example of the three benchmarks, the left subplot indicates that similar anatomical features are grouped together in the original medical images, as shown by the different anatomical regions in different colors.

label ratios. We use 2D UNet [64] as our backbone. Further implementation details are discussed in Appendix B.⁶

4.1. Main Results

In this subsection, we first examine whether our proposed ARCO can generalize well across various datasets and label ratios. Then, we investigate to what extent ARCO coupled with two samplers can realize two essential properties: (1) **model robustness**; and (2) **label efficiency**. The quantitative results for all the compared methods on three popular benchmarks (*i.e.*, ACDC [6], LiTS [8], MMWHS [98]) under various label ratios (*i.e.*, 1%, 5%, 10%) are collected in Tables 1, and 3 (Appendix D), respectively. Several consistent observations can be drawn from these extensive evaluations with sixteen segmentation networks.

① Superior Performance Across Datasets. We demonstrate that ARCO achieves superior performance across all datasets and label ratios. Specifically, our experiments consider three representative benchmarks (*i.e.*, ACDC [6], LiTS [8], MMWHS [98]) and different label ratios (*i.e.*, 1%, 5%, 10%). As shown in Tables 1, and 3 (Appendix D), we observe that our methods consistently outperform all the compared SSL-based methods by a considerable margin across all datasets and label ratios, which validates the superior performance of our proposed methods in both segmentation accuracy and label efficiency. For example, compared to the second-best MONA, our ARCO-SG under {1%, 5%, 10%} label ratios achieves {4.7%, 1.6%, 0.3%}, {8.3%, 2.1%, 1.2%}, {3.4%, 2.3%, 2.4%} in Dice across ACDC, LiTS, and MMWHS, respectively. Our ARCO-SAG achieves {4.3%, 1.2%, 0.2%}, {7.0%, 1.6%, 0.5%}, {2.2%, 3.0%, 2.3%} in Dice across ACDC, LiTS, and MMWHS. These results indicate that our methods can generalize to different clinical scenarios and label ratios.

② Across Label Ratios and Robustified Methods. To further validate the label efficiency property of our ARCO, we evaluate our ARCO-SG and ARCO-SAG with limited labeled training data available (*e.g.*, 1% and 5%). As demonstrated in Tables 1 and 3 (Appendix D), our models

under 5% label ratios surpass all the compared SSL methods by a significant performance margin. For example, compared to MONA, we observe our methods to push the best segmentation accuracy higher by 1.2% ~ 3.0% in Dice on ACDC, LiTS, and MMWHS, respectively. For example, the best segmentation accuracy on MMWHS rises from 86.3% to 89.3%. This suggests that our SSL-based approaches – without compromising the best achievable segmentation results – robustly improve performance using very limited labels, and further leads to a much-improved trade-off between SSL schemes and supervised learning schemes by avoiding a large amount of labeled data.

Similar to our results under 5% label ratio, our ARCO-SG and ARCO-SAG trained with 1% label ratio demonstrate sufficient performance boost compared to MONA by an especially significant margin, with up to 3.4% ~ 8.3% relative improvement in Dice. Taking the extremely limited label ratio (*i.e.*, 1%) as an indicator: (1) on ACDC, ARCO-SG achieves 4.7% higher average Dice, and 1.05 lower average ASD than the second best MONA; (2) on LiTS, ARCO-SG achieves 8.3% higher average Dice, and 1.7 lower average ASD than the second best MONA; and (3) considering the more challenging clinical scenarios (*i.e.*, 7 anatomical classes), ARCO-SG achieves 3.4% higher average Dice, and 3.27 lower average ASD than the second-best MONA on MMWHS. It highlights the superior performance of ARCO is not only from improved label efficiency but also credits to the superior model robustness.

③ Qualitative Results. We provide qualitative illustrations of ACDC and LiTS in Figures 4 and 6 (Appendix D.1), respectively. As shown in Figure 4, we observe that ARCO appears a significant advantage, where the edges and the boundaries of different anatomical regions are clearly more pronounced, such as RV and Myo regions. More interestingly, we found that in Figure 6, though all methods may confuse ambiguous tail-class samples such as small lesions, ARCO-SG and ARCO-SAG still produces consistently sharp and accurate object boundaries compared to the current approaches. We also observe similar results for ARCO on MMWHS in Figure 7 (Appendix D.2), where our approaches can regularize the segmentation results to

⁶We provide the PyTorch-like pseudo-code of our method in the supplementary material. Codes will be available upon the publication.

Table 1. Comparison results across the three labeled ratio settings (1%, 5%, 10%) on the ACDC and LiTS benchmarks. Best and second-best results are coloured **blue** and **red**, respectively. Please refer to the text for discussion.

Method	ACDC						LiTS					
	1% Labeled		5% Labeled		10% Labeled		1% Labeled		5% Labeled		10% Labeled	
	DSC ↑	ASD ↓	DSC ↑	ASD ↓	DSC ↑	ASD ↓	DSC ↑	ASD ↓	DSC ↑	ASD ↓	DSC ↑	ASD ↓
UNet-F [64]	91.5	0.996	91.5	0.996	91.5	0.996	68.5	17.8	68.5	17.8	68.5	17.8
UNet-L	14.5	19.3	51.7	13.1	74.4	2.20	57.0	34.6	60.4	30.4	61.6	28.3
EM [75]	21.1	21.4	59.8	5.64	75.7	2.73	56.6	38.4	61.2	33.3	62.9	38.5
CCT [60]	30.9	28.2	59.1	10.1	75.9	3.60	52.4	52.3	60.6	48.7	63.8	31.2
DAN [93]	34.7	25.7	56.4	15.1	76.5	3.01	57.2	27.1	62.3	25.8	63.2	30.7
URPC [53]	32.2	26.9	58.9	8.14	73.2	2.68	55.5	34.6	62.4	37.8	63.0	43.1
DCT [61]	36.0	24.2	58.5	10.8	78.1	2.64	57.6	38.5	60.8	34.4	61.9	31.7
ICT [74]	35.8	21.3	59.0	4.59	75.1	0.898	58.3	32.2	60.1	39.1	62.5	32.4
MT [68]	36.8	19.6	58.3	11.2	80.1	2.33	56.7	34.3	61.9	40.0	63.3	26.2
UAMT [89]	35.2	24.3	61.0	7.03	77.6	3.15	57.8	41.9	61.0	47.0	62.3	26.0
CPS [24]	37.1	30.0	61.0	2.92	78.8	3.41	57.7	39.6	62.1	36.0	64.0	23.6
GCL [15]	59.7	14.3	70.6	2.24	87.0	0.751	59.3	29.5	63.3	20.1	65.0	37.2
SCS [42]	59.4	12.7	73.6	5.37	84.2	2.01	57.8	39.6	61.5	28.8	64.6	33.9
PLC [16]	58.8	15.1	70.6	2.67	87.3	1.34	56.6	41.6	62.7	26.1	68.2	16.9
ACTION [85]	81.0	3.45	87.5	1.12	89.7	0.736	61.0	24.5	66.8	17.7	67.7	20.4
MONA [84]	82.6	2.03	88.8	0.624	90.7	0.864	64.1	20.9	67.3	16.4	69.3	18.0
• ARCO-SAG (ours)	87.0	0.986	90.0	0.810	90.9	0.570	71.1	20.6	68.9	13.2	69.8	13.5
◦ ARCO-SG (ours)	87.3	0.981	90.4	0.566	91.0	0.403	72.4	19.2	69.4	11.3	70.5	10.9

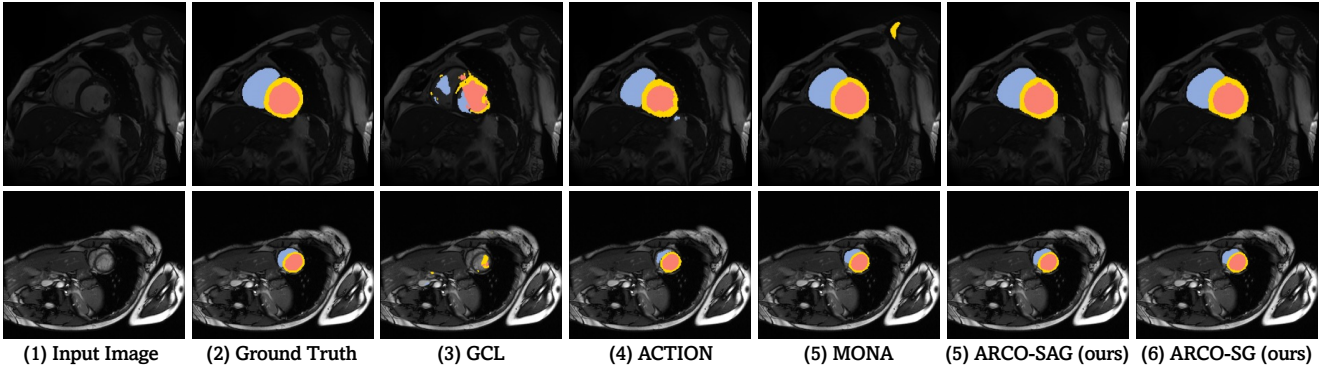


Figure 4. Visual comparisons with other methods on ACDC with 1% label ratio. As is shown, ARCO consistently produce more accurate predictions on anatomical regions and boundaries compared to all other SSL methods. Different anatomical regions are in different colors (RV: ■; Myo: ■; LV: ■).

be smooth and shape-consistent. Our findings suggest that ARCO improves model robustness mainly through distinguishing the minority tail-class samples.

4.2. Ablation Studies

In this subsection, we conduct various ablations to better understand our design choices. For all the ablation experiments the models are trained on ACDC with 1% labeled ratio. All experiments have three independent runs with different random seeds.

Importance of Loss Components. We analyze several critical components of our method in the final performance and conduct comprehensive ablation studies to validate their necessity. At the heart of our method is the combination of three losses: $\mathcal{L}_{\text{contrast}}$ for *tailness*, \mathcal{L}_{eqv} for *consistency*, and \mathcal{L}_{nn} for *diversity* (See Section 3 for more details). We deactivate each component and then evaluate the resulting mod-

Table 2. Ablation on loss component: (1) tailness; (2) consistency; (3) diversity, compared to the Vanilla and our methods.

Method	Metrics	
	Dice[%] ↑	ASD[mm] ↓
Vanilla	49.3	7.11
w/ tailness-SAG	79.7	0.827
w/ tailness-SG	80.2	0.698
w/ consistency	81.5	2.78
w/ diversity	62.8	3.97
w/ tailness-SAG + consistency	84.7	1.13
w/ tailness-SG + consistency	85.8	0.993
w/ consistency + diversity	81.8	3.29
w/ tailness-SAG + diversity	83.0	1.13
w/ tailness-SG + diversity	84.2	0.942
• ARCO-SAG (ours)	87.0	0.986
◦ ARCO-SG (ours)	87.3	0.981

els, as shown in Table 2. These results shows that each loss

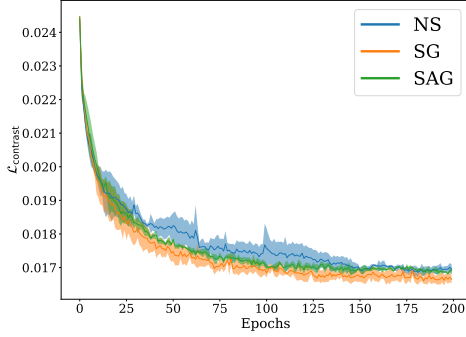


Figure 5. Visualization of training trajectories given by $\mathcal{L}_{\text{contrast}}$ vs. epochs on ACDC under 1% label ratio. The proposed ARCO is compared in terms of different sampling methods: Naïve Sampling (NS), Stratified Group (SG) Sampling, and Stratified-Antithetic Group (SAG) Sampling. The solid line and shaded area of each sampling method denote the mean and variance of test accuracies over 3 independent trials. Clearly, we observe SG sampling consistently outperforms the other sampling methods in convergence speed and training stability. SAG slightly outperforms NS.

component systematically boosts performance by a large margin, which suggests improved robustness.

Stability Analyses. In Figure 5, we show the stability analysis results on ARCO over different sampling methods. As we can see, our SG and SAG sampling facilitates convergence during the training. More importantly, SG sampling has stable performance with small standard derivations, which aligns with our hypothesis that our proposed sampling method can be viewed as the form of variance regularization. Moreover, loss landscape visualization of different loss functions (Figure 3) reveals similar conclusions.

Extra Study. More investigations about (1) generalization across label ratios and frameworks; (2) final checkpoint loss landscapes; (3) importance of augmentations; (4) ablation on different training settings are in Appendix E.

5. Conclusion

In this paper, we propose **ARCO**, a new semi-supervised contrastive learning framework for improved model robustness and label efficiency in medical image segmentation. Specifically, we propose two practical solutions via stratified group sampling theory that correct for the variance introduced by the common sampling practice, and achieve significant performance benefits. Our theoretical findings indicate Stratified Group and Stratified-Antithetic Group Sampling provide practical means for reducing variance. It presents a curated and easily adaptable training toolkit for training deep networks that generalize well beyond training data in those long-tail clinical scenarios. Future work includes exploring the benefit of ARCO in other medical image analysis application scenarios.

References

- [1] Zeyuan Allen-Zhu. How to make the gradients small stochastically: Even faster convex and nonconvex sgd. In *NeurIPS*, 2018.
- [2] Søren Asmussen and Peter W Glynn. *Stochastic simulation: algorithms and analysis*, volume 57. Springer, 2007.
- [3] Philip Bachman, Ouais Alsharif, and Doina Precup. Learning with pseudo-ensembles. In *NeurIPS*, 2014.
- [4] Wenjia Bai, Ozan Oktay, Matthew Sinclair, Hideaki Suzuki, Martin Rajchl, Giacomo Tarroni, Ben Glocker, Andrew King, Paul M Matthews, and Daniel Rueckert. Semi-supervised learning for network-based cardiac mr image segmentation. In *MICCAI*, 2017.
- [5] Adrien Bardes, Jean Ponce, and Yann LeCun. Vircreg: Variance-invariance-covariance regularization for self-supervised learning. *arXiv preprint arXiv:2105.04906*, 2021.
- [6] Olivier Bernard, Alain Lalonde, Clement Zotti, Frederick Cervenansky, Xin Yang, Pheng-Ann Heng, Irem Cetin, Karim Lekadir, Oscar Camara, Miguel Angel Gonzalez Ballester, et al. Deep learning techniques for automatic MRI cardiac multi-structures segmentation and diagnosis: Is the problem solved? *IEEE Transactions on Medical Imaging*, 2018.
- [7] Dimitri P Bertsekas and John N Tsitsiklis. Gradient convergence in gradient methods with errors. *SIAM Journal on Optimization*, 10(3):627–642, 2000.
- [8] Patrick Bilic, Patrick Ferdinand Christ, Eugene Vorontsov, Grzegorz Chlebus, Hao Chen, Qi Dou, Chi-Wing Fu, Xiao Han, Pheng-Ann Heng, Jürgen Hesser, et al. The liver tumor segmentation benchmark (lits). *arXiv preprint arXiv:1901.04056*, 2019.
- [9] Charles Blundell, Julien Cornebise, Koray Kavukcuoglu, and Daan Wierstra. Weight uncertainty in neural network. In *ICML*, 2015.
- [10] Gerda Bortsova, Florian Dubost, Laurens Hogeweg, Ioannis Katramados, and Marleen de Bruijne. Semi-supervised medical image segmentation via learning consistency under transformations. In *MICCAI*, 2019.
- [11] Léon Bottou, Frank E Curtis, and Jorge Nocedal. Optimization methods for large-scale machine learning. *Siam Review*, 60(2):223–311, 2018.
- [12] Robin Camarasa, Daniel Bos, Jeroen Hendrikse, Paul Nederkoorn, Eline Kooi, Aad van der Lugt, and Marleen de Bruijne. Quantitative comparison of monte-carlo dropout uncertainty measures for multi-class segmentation. *Uncertainty for Safe Utilization of Machine Learning in Medical Imaging, and Graphs in Biomedical Image Analysis*, 2020.
- [13] Hu Cao, Yueyue Wang, Joy Chen, Dongsheng Jiang, Xiaopeng Zhang, Qi Tian, and Manning Wang. Swin-unet: Unet-like pure transformer for medical image segmentation. *arXiv preprint arXiv:2105.05537*, 2021.
- [14] Xuyang Cao, Houjin Chen, Yanfeng Li, Yahui Peng, Shu Wang, and Lin Cheng. Uncertainty aware temporal-ensembling model for semi-supervised abus mass segmentation. *IEEE Transactions on Medical Imaging*, 2020.
- [15] Krishna Chaitanya, Ertunc Erdil, Neerav Karani, and Ender Konukoglu. Contrastive learning of global and local features

- for medical image segmentation with limited annotations. In *NeurIPS*, 2020.
- [16] Krishna Chaitanya, Ertunc Erdil, Neerav Karani, and Ender Konukoglu. Local contrastive loss with pseudo-label based self-training for semi-supervised medical image segmentation. *arXiv preprint arXiv:2112.09645*, 2021.
 - [17] Jieneng Chen, Yongyi Lu, Qihang Yu, Xiangde Luo, Ehsan Adeli, Yan Wang, Le Lu, Alan L Yuille, and Yuyin Zhou. Transunet: Transformers make strong encoders for medical image segmentation. In *MICCAI*, 2021.
 - [18] Liang Chen, Paul Bentley, Kensaku Mori, Kazunari Misawa, Michitaka Fujiwara, and Daniel Rueckert. Drinet for medical image segmentation. *IEEE Trans. Med. Imaging*, 2018.
 - [19] Liang-Chieh Chen, George Papandreou, Iasonas Kokkinos, Kevin Murphy, and Alan L Yuille. Deeplab: Semantic image segmentation with deep convolutional nets, atrous convolution, and fully connected crfs. *IEEE transactions on pattern analysis and machine intelligence*, 2017.
 - [20] Liang-Chieh Chen, Yukun Zhu, George Papandreou, Florian Schroff, and Hartwig Adam. Encoder-decoder with atrous separable convolution for semantic image segmentation. In *ECCV*, 2018.
 - [21] Ting Chen, Simon Kornblith, Mohammad Norouzi, and Geoffrey Hinton. A simple framework for contrastive learning of visual representations. In *ICML*, 2020.
 - [22] Ting Chen, Calvin Luo, and Lala Li. Intriguing properties of contrastive losses. In *NeurIPS*, 2021.
 - [23] Xinlei Chen and Kaiming He. Exploring simple siamese representation learning. In *CVPR*, 2021.
 - [24] Xiaokang Chen, Yuhui Yuan, Gang Zeng, and Jingdong Wang. Semi-supervised semantic segmentation with cross pseudo supervision. In *CVPR*, 2021.
 - [25] William G Cochran. *Sampling techniques*. John Wiley & Sons, 1977.
 - [26] Wenhui Cui, Yanlin Liu, Yuxing Li, Menghao Guo, Yiming Li, Xiuli Li, Tianle Wang, Xiangzhu Zeng, and Chuyang Ye. Semi-supervised brain lesion segmentation with an adapted mean teacher model. In *MICCAI*, 2019.
 - [27] Jifeng Dai, Haozhi Qi, Yuwen Xiong, Yi Li, Guodong Zhang, Han Hu, and Yichen Wei. Deformable convolutional networks. In *CVPR*, 2017.
 - [28] Alexey Dosovitskiy, Lucas Beyer, Alexander Kolesnikov, Dirk Weissenborn, Xiaohua Zhai, Thomas Unterthiner, Mostafa Dehghani, Matthias Minderer, Georg Heigold, Sylvain Gelly, et al. An image is worth 16x16 words: Transformers for image recognition at scale. In *ICLR*, 2020.
 - [29] Deng-Ping Fan, Tao Zhou, Ge-Peng Ji, Yi Zhou, Geng Chen, Huazhu Fu, Jianbing Shen, and Ling Shao. Inf-net: Automatic covid-19 lung infection segmentation from ct images. *IEEE Transactions on Medical Imaging*, 2020.
 - [30] Kang Fang and Wu-Jun Li. Dmnet: difference minimization network for semi-supervised segmentation in medical images. In *MICCAI*, 2020.
 - [31] Gaurav Fotedar, Nima Tajbakhsh, Shilpa Ananth, and Xiaowei Ding. Extreme consistency: Overcoming annotation scarcity and domain shifts. In *MICCAI*, 2020.
 - [32] Yarin Gal and Zoubin Ghahramani. Dropout as a bayesian approximation: Representing model uncertainty in deep learning. In *ICML*, 2016.
 - [33] Yunhe Gao, Rui Huang, Ming Chen, Zhe Wang, Jincheng Deng, Yuanyuan Chen, Yiwei Yang, Jie Zhang, Chanjuan Tao, and Hongsheng Li. Focusnet: Imbalanced large and small organ segmentation with an end-to-end deep neural network for head and neck ct images. In *MICCAI*. Springer, 2019.
 - [34] Simon Graham, Hao Chen, Jevgenij Gamper, Qi Dou, Pheng-Ann Heng, David Snead, Yee Wah Tsang, and Nasir Rajpoot. Mild-net: Minimal information loss dilated network for gland instance segmentation in colon histology images. *Medical image analysis*, 2019.
 - [35] Yves Grandvalet and Yoshua Bengio. Semi-supervised learning by entropy minimization. *NeurIPS*, 2004.
 - [36] Hayit Greenspan, Bram Van Ginneken, and Ronald M Summers. Guest editorial deep learning in medical imaging: Overview and future promise of an exciting new technique. *IEEE Trans. Med. Imaging*, 2016.
 - [37] Jean-Bastien Grill, Florian Strub, Florent Altché, Corentin Tallec, Pierre Richemond, Elena Buchatskaya, Carl Doersch, Bernardo Avila Pires, Zhaohan Guo, Mohammad Gheshlaghi Azar, et al. Bootstrap your own latent-a new approach to self-supervised learning. In *NeurIPS*, 2020.
 - [38] Ran Gu, Guotai Wang, Tao Song, Rui Huang, Michael Aertsen, Jan Deprest, Sébastien Ourselin, Tom Vercauteren, and Shaoting Zhang. Ca-net: Comprehensive attention convolutional neural networks for explainable medical image segmentation. *IEEE Trans. Med. Imaging*, 2020.
 - [39] Raia Hadsell, Sumit Chopra, and Yann LeCun. Dimensionality reduction by learning an invariant mapping. In *CVPR*, 2006.
 - [40] Ali Hatamizadeh, Yucheng Tang, Vishwesh Nath, Dong Yang, Andriy Myronenko, Bennett Landman, Holger Roth, and Daguang Xu. Unetr: Transformers for 3d medical image segmentation. *arXiv preprint arXiv:2103.10504*, 2021.
 - [41] Kaiming He, Haoqi Fan, Yuxin Wu, Saining Xie, and Ross Girshick. Momentum contrast for unsupervised visual representation learning. In *CVPR*, 2020.
 - [42] Xinrong Hu, Dewen Zeng, Xiaowei Xu, and Yiyu Shi. Semi-supervised contrastive learning for label-efficient medical image segmentation. In *MICCAI*, 2021.
 - [43] Tianyu Hua, Wenxiao Wang, Zihui Xue, Sucheng Ren, Yue Wang, and Hang Zhao. On feature decorrelation in self-supervised learning. In *ICCV*, 2021.
 - [44] Ziyu Jiang, Tianlong Chen, Ting Chen, and Zhangyang Wang. Improving contrastive learning on imbalanced data via open-world sampling. In *NeurIPS*, 2021.
 - [45] Li Jing, Pascal Vincent, Yann LeCun, and Yuandong Tian. Understanding dimensional collapse in contrastive self-supervised learning. *arXiv preprint arXiv:2110.09348*, 2021.
 - [46] Alain Jungo and Mauricio Reyes. Assessing reliability and challenges of uncertainty estimations for medical image segmentation. In *MICCAI*, 2019.
 - [47] Alex Kendall and Yarin Gal. What uncertainties do we need in bayesian deep learning for computer vision? In *NeurIPS*, 2017.

- [48] Dong-Hyun Lee et al. Pseudo-label: The simple and efficient semi-supervised learning method for deep neural networks. In *Workshop on challenges in representation learning, ICML*, 2013.
- [49] Xiaomeng Li, Lequan Yu, Hao Chen, Chi-Wing Fu, Lei Xing, and Pheng-Ann Heng. Transformation-consistent self-ensembling model for semisupervised medical image segmentation. *IEEE Transactions on Neural Networks and Learning Systems*, 2020.
- [50] Tsung-Yi Lin, Priya Goyal, Ross Girshick, Kaiming He, and Piotr Dollár. Focal loss for dense object detection. In *ICCV*, 2017.
- [51] Jonathan Long, Evan Shelhamer, and Trevor Darrell. Fully convolutional networks for semantic segmentation. In *CVPR*, 2015.
- [52] Xiangde Luo, Jieneng Chen, Tao Song, and Guotai Wang. Semi-supervised medical image segmentation through dual-task consistency. In *AAAI*, 2020.
- [53] Xiangde Luo, Wenjun Liao, Jieneng Chen, Tao Song, Yinan Chen, Shichuan Zhang, Nianyong Chen, Guotai Wang, and Shaoting Zhang. Efficient semi-supervised gross target volume of nasopharyngeal carcinoma segmentation via uncertainty rectified pyramid consistency. In *MICCAI*, 2021.
- [54] Alireza Mehrtash, William M Wells, Clare M Tempny, Purang Abolmaesumi, and Tina Kapur. Confidence calibration and predictive uncertainty estimation for deep medical image segmentation. *IEEE transactions on medical imaging*, 2020.
- [55] Luke Metz, Niru Maheswaranathan, Jeremy Nixon, Daniel Freeman, and Jascha Sohl-Dickstein. Understanding and correcting pathologies in the training of learned optimizers. In *ICML*, 2019.
- [56] Tanya Nair, Doina Precup, Douglas L Arnold, and Tal Arbel. Exploring uncertainty measures in deep networks for multiple sclerosis lesion detection and segmentation. *Medical image analysis*, 2020.
- [57] Dong Nie, Yaozong Gao, Li Wang, and Dinggang Shen. Asdnet: Attention based semi-supervised deep networks for medical image segmentation. In *MICCAI*, 2018.
- [58] Ozan Oktay, Jo Schlemper, Loic Le Folgoc, Matthew Lee, Mattias Heinrich, Kazunari Misawa, Kensaku Mori, Steven McDonagh, Nils Y Hammerla, Bernhard Kainz, et al. Attention u-net: Learning where to look for the pancreas. *arXiv preprint arXiv:1804.03999*, 2018.
- [59] Aaron van den Oord, Yazhe Li, and Oriol Vinyals. Representation learning with contrastive predictive coding. *arXiv preprint arXiv:1807.03748*, 2018.
- [60] Yassine Ouali, Céline Hudelot, and Myriam Tami. Semi-supervised semantic segmentation with cross-consistency training. In *CVPR*, 2020.
- [61] Siyuan Qiao, Wei Shen, Zhishuai Zhang, Bo Wang, and Alan Yuille. Deep co-training for semi-supervised image recognition. In *ECCV*, 2018.
- [62] Maithra Raghu, Chiyuan Zhang, Jon Kleinberg, and Samy Bengio. Transfusion: Understanding transfer learning for medical imaging. In *NeurIPS*, 2019.
- [63] Simon Reiß, Constantin Seibold, Alexander Freytag, Erik Rodner, and Rainer Stiefelhagen. Every annotation counts: Multi-label deep supervision for medical image segmentation. In *CVPR*, 2021.
- [64] Olaf Ronneberger, Philipp Fischer, and Thomas Brox. U-net: Convolutional networks for biomedical image segmentation. In *MICCAI*, 2015.
- [65] Mehdi Sajjadi, Mehran Javanmardi, and Tolga Tasdizen. Regularization with stochastic transformations and perturbations for deep semi-supervised learning. In *NeurIPS*, 2016.
- [66] Henry Scudder. Probability of error of some adaptive pattern-recognition machines. *IEEE Trans. Inf. Theory*, 1965.
- [67] Gonglei Shi, Li Xiao, Yang Chen, and S Kevin Zhou. Marginal loss and exclusion loss for partially supervised multi-organ segmentation. *Medical Image Analysis*, 2021.
- [68] Antti Tarvainen and Harri Valpola. Mean teachers are better role models: Weight-averaged consistency targets improve semi-supervised deep learning results. In *NeurIPS*, 2017.
- [69] Ajinkya Tejankar, Soroush Abbasi Koohpayegani, Vipin Pillai, Paolo Favaro, and Hamed Pirsiavash. Isd: Self-supervised learning by iterative similarity distillation. In *ICCV*, 2021.
- [70] Yuandong Tian, Xinlei Chen, and Surya Ganguli. Understanding self-supervised learning dynamics without contrastive pairs. In *ICML*. PMLR, 2021.
- [71] Yonglong Tian, Chen Sun, Ben Poole, Dilip Krishnan, Cordelia Schmid, and Phillip Isola. What makes for good views for contrastive learning? *NeurIPS*, 2020.
- [72] Jeya Maria Jose Valanarasu, Poojan Oza, Ilker Hacihaliloglu, and Vishal M Patel. Medical transformer: Gated axial-attention for medical image segmentation. In *MICCAI*, 2021.
- [73] Ashish Vaswani, Noam Shazeer, Niki Parmar, Jakob Uszkoreit, Llion Jones, Aidan N Gomez, Łukasz Kaiser, and Illia Polosukhin. Attention is all you need. In *NeurIPS*, 2017.
- [74] Vikas Verma, Kenji Kawaguchi, Alex Lamb, Juho Kannala, Yoshua Bengio, and David Lopez-Paz. Interpolation consistency training for semi-supervised learning. In *IJCAI*, 2019.
- [75] Tuan-Hung Vu, Himalaya Jain, Maxime Bucher, Matthieu Cord, and Patrick Pérez. Advent: Adversarial entropy minimization for domain adaptation in semantic segmentation. In *CVPR*, 2019.
- [76] Yicheng Wu, Zongyuan Ge, Donghao Zhang, Minfeng Xu, Lei Zhang, Yong Xia, and Jianfei Cai. Mutual consistency learning for semi-supervised medical image segmentation. *Medical Image Analysis*, 2022.
- [77] Yicheng Wu, Yong Xia, Yang Song, Donghao Zhang, Dongnan Liu, Chaoyi Zhang, and Weidong Cai. Vessel-net: retinal vessel segmentation under multi-path supervision. In *MICCAI*, 2019.
- [78] Yicheng Wu, Yong Xia, Yang Song, Yanning Zhang, and Weidong Cai. Multiscale network followed network model for retinal vessel segmentation. In *MICCAI*, 2018.
- [79] Jinxi Xiang, Zhuowei Li, Wenji Wang, Qing Xia, and Shaoting Zhang. Self-ensembling contrastive learning for semi-supervised medical image segmentation. *arXiv preprint arXiv:2105.12924*, 2021.
- [80] Qizhe Xie, Minh-Thang Luong, Eduard Hovy, and Quoc V Le. Self-training with noisy student improves imagenet classification. In *CVPR*, 2020.

- [81] Yutong Xie, Jianpeng Zhang, Zehui Liao, Yong Xia, and Chunhua Shen. Pgl: prior-guided local self-supervised learning for 3d medical image segmentation. *arXiv preprint arXiv:2011.12640*, 2020.
- [82] Yutong Xie, Jianpeng Zhang, Chunhua Shen, and Yong Xia. Cotr: Efficiently bridging cnn and transformer for 3d medical image segmentation. In *MICCAI*, 2021.
- [83] Yuan Xue, Hui Tang, Zhi Qiao, Guanzhong Gong, Yong Yin, Zhen Qian, Chao Huang, Wei Fan, and Xiaolei Huang. Shape-aware organ segmentation by predicting signed distance maps. *arXiv preprint arXiv:1912.03849*, 2019.
- [84] Chenyu You, Weicheng Dai, Fenglin Liu, Haoran Su, Xiaoran Zhang, Lawrence Staib, and James S Duncan. Mine your own anatomy: Revisiting medical image segmentation with extremely limited labels. *arXiv preprint arXiv:2209.13476*, 2022.
- [85] Chenyu You, Weicheng Dai, Lawrence Staib, and James S Duncan. Bootstrapping semi-supervised medical image segmentation with anatomical-aware contrastive distillation. *arXiv preprint arXiv:2206.02307*, 2022.
- [86] Chenyu You, Ruihan Zhao, Fenglin Liu, Sandeep Chinchali, Ufuk Topcu, Lawrence Staib, and James S Duncan. Class-aware generative adversarial transformers for medical image segmentation. *arXiv preprint arXiv:2201.10737*, 2022.
- [87] Chenyu You, Ruihan Zhao, Lawrence Staib, and James S Duncan. Momentum contrastive voxel-wise representation learning for semi-supervised volumetric medical image segmentation. *arXiv preprint arXiv:2105.07059*, 2021.
- [88] Chenyu You, Yuan Zhou, Ruihan Zhao, Lawrence Staib, and James S Duncan. Simcvd: Simple contrastive voxel-wise representation distillation for semi-supervised medical image segmentation. *IEEE Transactions on Medical Imaging*, 2022.
- [89] Lequan Yu, Shujun Wang, Xiaomeng Li, Chi-Wing Fu, and Pheng-Ann Heng. Uncertainty-aware self-ensembling model for semi-supervised 3d left atrium segmentation. In *MICCAI*, 2019.
- [90] Jure Zbontar, Li Jing, Ishan Misra, Yann LeCun, and Stéphane Deny. Barlow twins: Self-supervised learning via redundancy reduction. In *ICML*. PMLR, 2021.
- [91] Dewen Zeng, Yawen Wu, Xinrong Hu, Xiaowei Xu, Haiyun Yuan, Meiping Huang, Jian Zhuang, Jingtong Hu, and Yiyu Shi. Positional contrastive learning for volumetric medical image segmentation. In *MICCAI*, 2021.
- [92] Yu Zeng, Yunzhi Zhuge, Huchuan Lu, and Lihe Zhang. Joint learning of saliency detection and weakly supervised semantic segmentation. In *ICCV*, 2019.
- [93] Yizhe Zhang, Lin Yang, Jianxu Chen, Maridel Fredericksen, David P Hughes, and Danny Z Chen. Deep adversarial networks for biomedical image segmentation utilizing unannotated images. In *MICCAI*, 2017.
- [94] Hengshuang Zhao, Jianping Shi, Xiaojuan Qi, Xiaogang Wang, and Jiaya Jia. Pyramid scene parsing network. In *CVPR*, 2017.
- [95] Heliang Zheng, Jianlong Fu, Zheng-Jun Zha, and Jiebo Luo. Learning deep bilinear transformation for fine-grained image representation. In *NeurIPS*, 2019.
- [96] Yanning Zhou, Hao Chen, Huangjing Lin, and Pheng-Ann Heng. Deep semi-supervised knowledge distillation for overlapping cervical cell instance segmentation. In *MICCAI*, 2020.
- [97] Yuyin Zhou, Yan Wang, Peng Tang, Song Bai, Wei Shen, Elliot Fishman, and Alan Yuille. Semi-supervised 3d abdominal multi-organ segmentation via deep multi-planar co-training. In *WACV*, 2019.
- [98] Xiahai Zhuang and Juan Shen. Multi-scale patch and multi-modality atlases for whole heart segmentation of mri. *Medical image analysis*, 2016.